Semnan University

Journal of Modeling & Simulation in Electrical & Electronics Engineering (MSEEE)

Journal homepage: **https://mseee.semnan.ac.ir/**

ISSN: 2821-0786

A Novel 70 GHz Circularly Polarized Fully-Planar Leaky-Wave Antenna with X-shaped slots for Millimeter-Wave Radar Applications

Yalda Torabi [1*]

***Abstract*- This paper presents a novel, fully planar circularly polarized periodic leaky-wave antenna (CP-PLWA) designed for wide-beam scanning in the 70 GHz band for millimeter-wave radar applications. A complementary split ring resonator half-mode substrate integrated waveguide (CSRR-HMSIW) feed structure is employed, offering a low-loss, and readily manufacturable implementation. The key innovation is the integration of cascaded X-shaped slots within the radiating patch, which facilitates controlled surface current perturbation and optimized excitation of orthogonal E-field components, resulting in a significantly enhanced circular polarization bandwidth. This design enables backward-to-forward beam scanning while maintaining a fully planar, via-free architecture. Simulated results demonstrate a 20.1% impedance bandwidth (64.4–77.75 GHz), an axial ratio bandwidth exceeding 13.6% (66–75 GHz, AR < 3 dB), and a wide scan angle from –15° to +60°. A gain exceeding 13 dBi (peaking at 16 dBi) is achieved with a simulated radiation efficiency greater than 97%. This compact, fully planar design, fabricated on a Rogers RT/duroid 5880 substrate, advances the state-of-the-art in CP LWAs for 70 GHz millimeter-wave radar systems by simultaneously addressing critical limitations of prior art: achieving wide CP bandwidth in a planar configuration, eliminating fabrication-via complexity, and maintaining high efficiency across a wide scanning range. The proposed antenna offers a promising solution for future high-performance radar applications requiring compact, wideband, and frequency-scanned circularly polarized radiation.**

***Index Terms:* Circularly-Polarized (CP), Leaky-Wave Antenna (LWA), Half-Mode Substrate Integrated Waveguide (HMSIW), 70 GHz band, Wide-Beam Scanning, Planar, Metamaterial, CSRR.**

I. Introduction

Millimeter-wave (mm-wave) frequencies have emerged as essential for next-generation wireless systems, supporting multi-gigabit data rates in 5G/6G networks [1] while enabling high-resolution sensing for automotive and security applications[2]. The integration of communication and radar functionalities in these bands requires antennas with exceptional performance metrics, including wide bandwidth, high gain, and frequency-agile beam steering [3].

Within the mm-wave spectrum, the 70 GHz band presents distinct advantages over the adjacent 60 GHz band, which suffers from high atmospheric attenuation due to oxygen absorption [4]. The 70 GHz window offers relatively lower path loss while maintaining the benefits of a wide available bandwidth, making it increasingly attractive for both communication and radar applications [5].

To exploit this potential, Leaky-Wave Antennas (LWAs) have emerged as a leading candidate. Unlike complex phased arrays that require costly phase shifters, LWAs possess the unique ability to steer the main beam continuously from backward to forward angles simply by sweeping frequency [6-10]. This inherent frequency-scanning capability allows for simplified, high-gain, and low-cost radar architectures perfectly suited for mass production.

Substrate integrated waveguide (SIW) technology has emerged as a promising platform for mm-wave antenna design, combining the advantages of rectangular waveguides with planar circuit fabrication [11]. SIW-based leaky-wave antennas (LWAs) are particularly attractive for frequency-scanning applications due to their inherent beam-steering

Received; 2025-12-11 Revised; 2026-02-05 Accepted; 2026-02-22

1. Electrical Engineering Department, University of Zanjan, Zanjan, Iran.
*Corresponding author: y.torabi@znu.ac.ir

Cite this article as:
Torabi, Y. (2026). A Novel 70 GHz Circularly Polarized Fully-Planar Leaky-Wave Antenna with X-shaped slots for Millimeter-Wave Radar Applications. *Journal of Modeling & Simulation in Electrical & Electronics Engineering (MSEEE)*. Semnan University Press. 6 (2), 33-41.
DOI: https://doi.org/10.22075/MSEEE.2026.40021.1241

capability, high directivity, and relatively simple feeding structures [12, 13]. The half-mode SIW (HMSIW) variant further reduces the antenna footprint by approximately 50% while preserving most electrical characteristics, enabling more compact designs [14, 15].

However, a critical limitation in existing LWA technology restricts its practical deployment in modern radar systems. Radar systems operate in dynamic environments where Circular Polarization (CP) is mandatory to suppress multi-path interference and mitigate polarization mismatch losses [16]. Linear Polarization (LP), unfortunately, is susceptible to severe signal fading in these scenarios.

This creates a significant gap in the current state of the art, characterized by a trade-off between structural simplicity and polarization performance. For instance, while recent PCB-based LWAs have achieved compact footprints and beam scanning [17, 18], they are predominantly limited to LP, rendering them less effective for robust sensing applications despite their structural advantages.

Conversely, designs that successfully achieve wideband Circular Polarization often resort to bulky 3D-printed structures [19] or complex multi-layer technologies like Continuous Transverse Stub (CTS) arrays [20], which negate the low-profile and low-cost advantages required for mass production. Although some dielectric-based antennas have successfully demonstrated CP radiation [16], they typically exhibit a severely restricted scanning range (e.g., less than 20°), limiting their field of view.

Furthermore, the realization of fully planar CP structures at 70 GHz remains a formidable challenge. Conventional SIW designs rely on metallic vias, which introduce fabrication complexity and increased losses at these frequencies. While earlier attempts to utilize metamaterial-inspired structures, such as Complementary Split-Ring Resonators (CSRRs) or Complementary Electrical LC Resonators (CELCs), have demonstrated the feasibility of planar via-free designs [21, 22], these initial explorations were often constrained by limited axial-ratio bandwidths, moderate gain levels, and a lack of a systematic analytical design framework, leaving a significant gap for high-efficiency, wide-scanning planar solutions.

Addressing these limitations, this paper presents a novel 70 GHz fully planar CP HMSIW LWA that fundamentally departs from prior resonator-loaded designs. The core innovation lies in the introduction of cascaded X-shaped slots within the radiating aperture. Unlike standard slots or CELC resonators used in earlier literature, the proposed X-shaped topology provides a superior degree of freedom for controlling orthogonal current modes. This geometric innovation enables a simultaneous breakthrough in performance metrics: achieving a record-wide axial ratio bandwidth (>13.6%), a high peak gain of 16 dBi, and a broad scanning range of 75° (-15° to +60°). A key advancement is the provided comprehensive design framework, which details the HMSIW derivation, CRLH balance conditions, and the analytical relationship between X-slot geometry and CP performance-a systematic approach absent in prior optimization-based works. By eliminating metallic vias and optimizing the slot configuration, the proposed design successfully synthesizes the high performance of bulky antennas with the simplicity of planar fabrication, offering a robust solution for future mm-wave radar applications.

The paper is structured as follows: Section II details the antenna geometry and design methodology. Section III presents simulated results. Section IV provides a state-of-the-art comparison. Section V discusses fabrication challenges, and Section VI concludes the work.

II. Antenna Geometry, Design Theory and Analytical Framework Design

The proposed Circularly Polarized Periodic Leaky-Wave Antenna (CP-PLWA) is depicted in Fig. 1(a). Its core is a fully planar, via-free feed line based on the Complementary Split-Ring Resonator Half-Mode Substrate Integrated Waveguide (CSRR-HMSIW) concept. The key innovation lies in integrating cascaded X-shaped slots within the radiating patch to achieve wideband circular polarization. This section details the design evolution, analytical framework, and final optimized parameters.

A. Unit Cell Configuration and Design Evolution

The fundamental building block of the proposed leaky-wave antenna is a periodic unit cell based on a modified HMSIW structure. As illustrated in Fig. 1(b), the unit cell consists of three key components: (1) a planar HMSIW line where the conventional metallic via sidewall is replaced by a broadside-coupled CSRR array; (2) two horizontal stubs extending from the main patch; and (3) three cascaded X-shaped slots etched into the patch surface. This configuration achieves a fully planar, via-free structure while providing the necessary electromagnetic properties for circular polarization and beam.

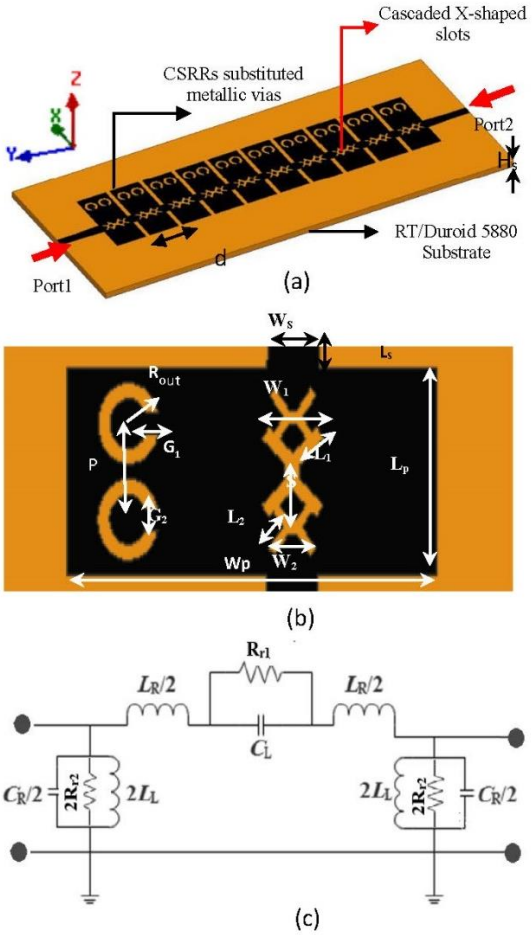

Fig.1. Geometry of the proposed CP-LWA based on CSRR-HMSIW technology: (a) Perspective view of the complete periodic antenna, (b) Top view of the single unit cell with design parameters, and (c) Corresponding equivalent LC circuit model.

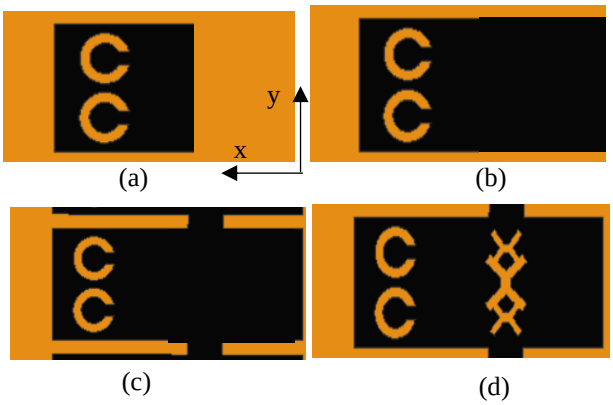

Fig. 2. Design evolution of the CRLH unit cell: (a) Initial CSRR-HMSIW structure; (b) Widened topology for asymmetric elliptical polarization with a dominant E_x component; (c) Introduction of horizontal stubs (inter-cell gaps) to generate the E_y component with a 90° phase shift; and (d) Integration of cascaded X-shaped slots to enhance CP performance.

scanning.

To achieve backward-to-forward beam scanning, the structure is designed as a composite right/left-handed (CRLH) transmission line. The equivalent circuit model of the unit cell (Fig. 1 (c)) comprises right-handed (RH) elements L_R and C_R from the HMSIW line, and left-handed (LH) elements C_L and L_L realized by the inter-cell gaps and CSRRs, respectively. Furthermore, from the radiation viewpoint, most of the radiation occurs along the edges of inter-cell gaps and the open side of CSRR-HMSIW, which are represented by (R_{r1}) and (R_{r2}), respectively.

To achieve backward-to-forward scanning and CP radiation, the design evolves from a basic symmetric CSRR-HMSIW (Fig. 2(a)) through three modifications. First, the cavity width is expanded (Fig. 2(b)) to break longitudinal symmetry, exciting a dominant transverse field (E_x) via shunt radiation. Second, horizontal stubs are introduced (Fig. 2 (c)) to form distinct inter-cell gaps; these serve dual purposes by providing the series capacitance (C_L) for the LH mode and radiating the orthogonal longitudinal component (E_y). The intrinsic spatial offset between these shunt and series sources facilitates the quadrature phase difference required for circular polarization. Finally, cascaded X-shaped slots are etched (Fig. 2(d)) to modulate surface currents, balancing the orthogonal field magnitudes for wideband CP performance.

B. HMSIW Feed Design

The design begins with the HMSIW transmission line. For a substrate with relative permittivity ϵ_r and thickness H_s, the effective width W_{eff} required to achieve a specific cut-off frequency f_c for the dominant TE_{10} mode is given by the standard HMSIW relation [23]:

$$W_{eff} = \frac{c}{4f_c\sqrt{\varepsilon_{eff}}} \tag{1}$$

where c is the speed of light in vacuum and $\varepsilon_{eff} \approx (\varepsilon_r + 1)/2$ is the effective permittivity for the dominant mode of the HMSIW [24]. To guarantee single-mode operation over the 64–78 GHz band, the cut-off frequency is chosen as $f_c \approx 58$ GHz, following standard SIW/HMSIW design guidelines[25].

The physical patch width Wp is obtained by correcting the effective width to account for fringing fields at the open boundary of the HMSIW [26]:

$$W_p = W_{eff} - \Delta W \tag{2}$$

For a thin substrate, the fringing field extension ΔW can be approximated using the classical microstrip edge correction model [27]:

$$\Delta W \approx \frac{H_s}{\pi}\left[\ln\left(\frac{2H_s}{t}\right) + 1\right] \tag{3}$$

where t denotes the metallization thickness. The resulting physical width obtained from Eqs. (1)– (3) serve as an initial baseline. In the proposed antenna, however, the final patch width is deliberately increased to $W_p = 2.8\,mm$ through explicit electromagnetic optimization. This intentional widening breaks the longitudinal symmetry (Fig. 2(b)), enhances radiation from the open edge, and enables the generation of circular polarization. The patch length L_p is set to 1.5 mm according to the unit-cell periodicity constraints.

C. CSRR Wall Design and Resonance Analysis

The CSRR array functions as an effective electric wall. The fundamental resonance frequency of an individual circular CSRR unit is governed by its equivalent inductance (L_{CSRR}) and capacitance (C_{CSRR}). For a CSRR with outer radius R_{out}, ring width G_1, and gap G_2, these parameters are initially estimated using the analytical expressions reported in [28]:

$$f_{\mathrm{res}} = \frac{1}{2\pi\sqrt{L_{\mathrm{CSRR}}\,C_{\mathrm{CSRR}}}} \tag{4}$$

The inductance is mainly associated with the magnetic current loop of the resonator and can be approximated using the classical circular loop inductance expression [29], as adopted for CSRR structures in [28]:

$$L_{CSRR} \approx \mu_0\pi R_{\mathrm{out}}\left[\ln\left(\frac{8R_{\mathrm{out}}}{G_1 + G_2}\right) - 2\right] \tag{5}$$

The equivalent capacitance arises from the split gap and the fringing electric fields between the inner and outer rings. Following the gap-capacitance model and the physical interpretation of CSRRs reported in [28, 30], the capacitance can be approximated as:

$$C_{CSRR} \approx \varepsilon_0\varepsilon_{eff}\frac{\pi(R_{\mathrm{out}} - G_1/2)G_2}{G_1} \tag{6}$$

Starting from these analytical estimates, the CSRR geometry is subsequently refined through full-wave electromagnetic optimization. The optimized dimension values ($R_{\mathrm{out}} = 0.3\,mm$, G_1=0.12 mm, G_2=0.15 mm, inter-CSRR spacing p=0.5 mm), place the array's stopband below the operating frequency, ensuring that it behaves as a high-impedance wall within the 64–78 GHz band.

D. CRLH Metamaterial Implementation and Balance Condition

To enable continuous backward-to-forward scanning, the unit cell is designed as a balanced CRLH transmission line (Fig. 1 (c)). The inherent HMSIW structure provides the right-handed parameters (L_R, C_R), while the CSRR array contributes the shunt LH inductance (L_L).

To realize the series Left-Handed capacitance (C_L), the unit cells are separated by a gap defined by the stub lengths. While the central narrow bridge (width W_s) provides the inductive

connection, the dominant series capacitance is formed by the coupling between the adjacent edges of the main radiating patches. The effective gap distance between the main patches is approximately ($g \approx 2L_s$). Consequently, the series capacitance can be analytically approximated as the gap capacitance between two microstrip lines [31]:

$$C_L \approx \varepsilon_0 \varepsilon_{eff} \frac{L_s(W_P - W_s)}{2l_s} K_f \quad (7)$$

where W_P is the main patch width, W_s is the connecting bridge width, and $2L_S$ represents the physical separation between the patch edges. The term ($W_P - W_s$) represents the effective coupling length of the patch edges. K_f is a correction factor accounting for the fringing fields through the air and substrate, which dominate the coupling due to the thin metallization.

The optimized dimensions for the coupling structure are $L_s = 0.2\ mm$ and W_s=0.5 mm (stub dimensions) .

The shunt LH inductance L_L is provided by the CSRR wall. Its value is related to the CSRR's equivalent inductance:

$$L_L \approx L_{CSRR} \quad (8)$$

The RH inductance L_R and capacitance C_R are inherent to the HMSIW section of length *d* (the unit cell period) [31]:

$$L_R \approx \frac{Z_0\sqrt{\varepsilon_{eff}}d}{c} \text{ and } C_R \approx \frac{d\sqrt{\varepsilon_{eff}}}{Z_0 c} \quad (9)$$

where Z_0 is the characteristic impedance of the HMSIW line.

The fundamental requirement for continuous scanning through broadside without an open stopband is the balanced condition of the CRLH unit cell:

$$L_R C_L = L_L C_R \quad (10)$$

This condition ensures the phase constant $\beta = 0$ at the target broadside frequency f_0=67 GHz. Eq. (10) served as the key analytical constraint during the parametric optimization process, guiding the adjustment of stub dimensions (L_s, W_s), gap (g), and CSRR parameters to achieve the desired balance.

E. Circular Polarization Mechanism and X-Slot Design

CP generation relies on the excitation of orthogonal modes with a quadrature phase shift. The widened cavity breaks longitudinal symmetry, creating a dominant transverse E_x component (shunt radiation), while the inter-cell gaps radiate the orthogonal E_y component (series radiation). The physical displacement between these radiating apertures inherently provides the necessary 90° phase difference. Furthermore, cascaded X-shaped slots perturb the surface current path to equalize the amplitudes of E_x and E_y, significantly extending the operational CP bandwidth.

The initial slot dimensions are derived from the guided wavelength λ_g at the center frequency[31]:

$$L_1 \approx \frac{\lambda_g}{8} = \frac{c}{8f_0\sqrt{\varepsilon_{eff}}} \quad (11)$$

After full-wave optimization, the final optimized dimensions of the cascaded X-shaped slots are W_1=0.60 mm, W_2=0.15 mm, L_1=0.30 mm, L_2=0.21 mm, and S=0.5 mm. These parameters were optimized to achieve circular polarization with an axial ratio below 3 dB over the widest possible frequency range, resulting in a CP bandwidth of 66–75 GHz (13.6%). The cascaded slots enhance orthogonal mode excitation, phase control, and impedance bandwidth, thereby widening the CP bandwidth (axial ratio (AR) < 3 dB). Fig.3 illustrates the surface current (J_s) distribution on the radiating element at various time instants within one period, confirming CP generation via anticlockwise rotation.

1.1 F. Complete Antenna Configuration and Dispersion Analysis

The complete CP-PLWA consists of N=10 identical unit cells arranged with a period *d*. Radiation occurs due to periodic perturbation of the CSRR-HMSIW field, exciting radiating space harmonics. The initial value of the period is obtained from the analytical broadside condition of CRLH leaky-wave antennas at the transition frequency f_0=67 GHz ($\beta = 0$) [31]:

$$d \approx \frac{\lambda_g}{2} = \frac{c}{2f_0\sqrt{\varepsilon_{eff}}} \quad (12)$$

which is subsequently refined through full-wave optimization, yielding an optimized period of d = 1.8 mm.

The propagation constant of the nth space harmonic is given by [31]:

$$\beta_n = \beta_0 + \frac{2\pi n}{d} \quad (13)$$

where β_0 is the fundamental mode constant. Radiation occurs when $|\beta_n/K_0| \leq 1$. In this design, the n=−1 harmonic is the dominant radiating mode. The main beam angle θ is therefore approximated by[31]:

$$\theta \approx \sin^{-1}\left(\frac{\beta_{-1}}{k_0}\right) \quad (14)$$

The dispersion characteristics (β and attenuation constant α) of the unit cell were extracted from a two-port full-wave simulation using the following relations [31]:

$$\beta = \frac{1}{d}\left|Im\left(cosh^{-1}\left(\frac{1 - S_{11}S_{22} + S_{12}S_{21}}{2S_{21}}\right)\right)\right| \quad (15)$$

$$\alpha = \frac{1}{d}\left|Re\left(cosh^{-1}\left(\frac{1 - S_{11}S_{22} + S_{12}S_{21}}{2S_{21}}\right)\right)\right| \quad (16)$$

The resulting dispersion diagram is shown in Fig. 4. A continuous transition at $\beta = 0$ occurs at f_0 = 67 GHz, indicating a balanced CRLH behavior and confirming the absence of an open stopband. Negative slope for f < f_0 corresponds to backward radiation, while positive slope for f > f_0 indicates forward radiation.

To clarify the radiation mechanism and frequency-dependent beam behavior, the electric field distribution of the proposed CP-PLWA is examined at two representative frequencies. At 67.15 GHz, corresponding to the broadside radiation condition (β = 0), the electric field exhibits a symmetric distribution along the antenna axis, indicating in-phase radiation from successive unit cells and confirming broadside beam formation. At 72 GHz, where β > 0, the field distribution shows a clear longitudinal phase progression, resulting in a tilted wavefront and forward beam radiation. At both frequencies, strong electric field concentration occurs around the edges of the cascaded X-shaped slots, confirming their role as the dominant radiating apertures.

III. RESULTS AND DISCUSSION

The electromagnetic performance of the proposed circularly polarized periodic leaky-wave antenna

(CP-PLWA) was investigated through full-wave simulations using Ansys HFSS. To ensure numerical robustness and enhance the credibility of the results in the absence of experimental validation, the key performance metrics were independently cross-verified using CST Microwave Studio. The results presented in this section correspond to the final optimized design and are consistent across both simulation platforms.

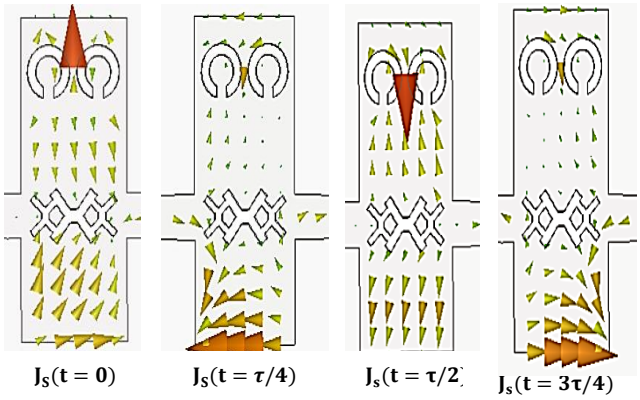

Fig. 3. Surface current (*Js*) distribution on the radiating element (70 GHz) over one period, confirming RHCP generation.

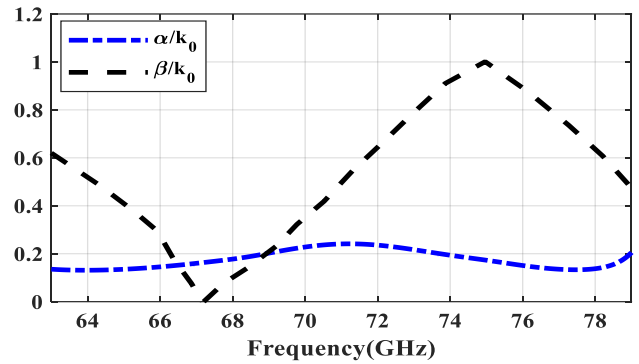

Fig. 4. Dispersion diagram for the unit cell of the proposed antenna, showing the balanced CRLH response with β=0 at 67.15 GHz.

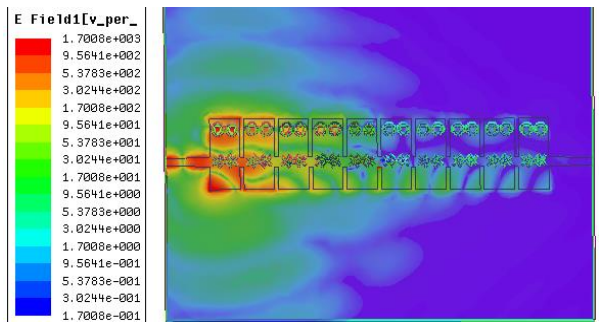

Fig. 5. 67.15 radiati the antenna axis, confirming forward leaky-wave radiation (β > 0).

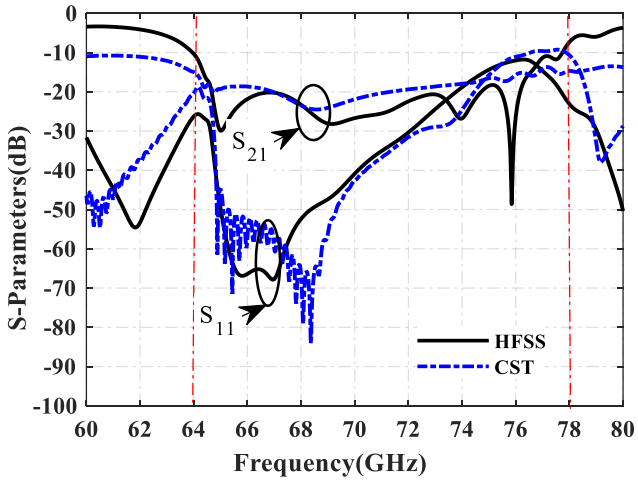

Fig. 6. S-Parameters of the proposed LWA.

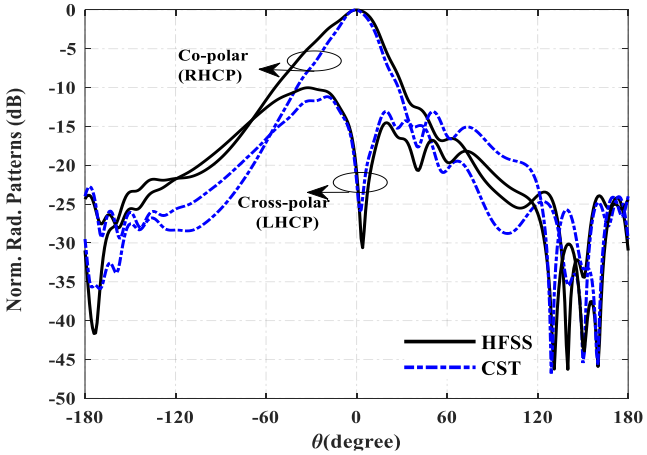

Fig. 7. Normalized co- and cross-polarized (RHCP and LHCP) radiation patterns at 67.15 GHz (YZ plane).

A. Impedance Characteristics and Traveling-Wave Behavior

Fig. 6 shows the simulated S-parameters of the proposed antenna. The reflection coefficient satisfies $|S_{11}|<-10$ dB over the frequency range from 64.4 to 77.75 GHz, corresponding to an impedance bandwidth of approximately 20.1%. The transmission coefficient $|S_{21}|$ remains below −20 dB across most of the operational band (65–75 GHz), indicating efficient power leakage through radiation rather than dissipation.

This behavior is characteristic of well-designed leaky-wave structures, where low reflection and transmission levels, combined with minimal dielectric and conductor losses, enable effective radiation from the periodic apertures. The close agreement between HFSS and CST results, with only minor discrepancies near the band edges, confirms the stable traveling-wave operation of the CSRR-HMSIW-based structure.

B. Radiation Characteristics at Broadside

The radiation performance at the broadside frequency is examined at 67.15 GHz, which corresponds to the balanced condition identified in the dispersion analysis. Fig.7 presents the normalized co-polarized (RHCP) and cross-polarized (LHCP) radiation patterns in the YZ plane, obtained from both HFSS and CST.

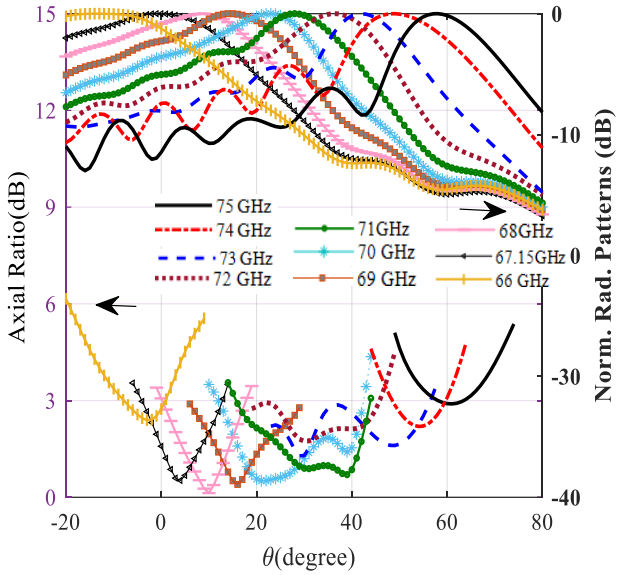

Fig. 8. Simulated normalized LHCP radiation patterns and corresponding axial ratio in the YZ plane at various frequencies.

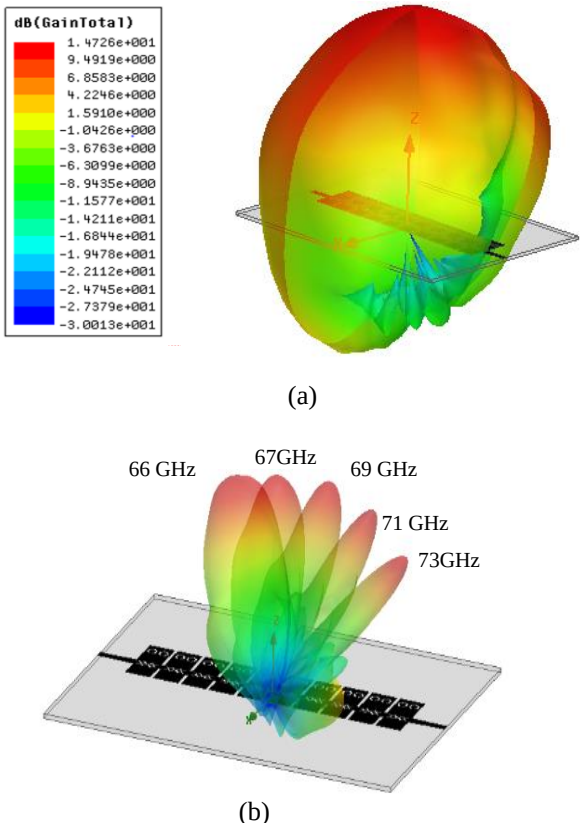

Fig. 9. 3D radiation patterns of the antenna: (a) broadside pattern at 67.15 GHz (dB scale), and (b) linear-scale patterns at 66, 67.15, 69, 73, and 73.21 GHz showing beam scanning with frequency.

The two solvers predict nearly identical radiation characteristics: the main beam is directed at 0°, and the cross-polarized component within the main lobe is suppressed by approximately 30 dB relative to the co-polarized component. This high level of polarization purity confirms the effective excitation of circular polarization at broadside and validates the perturbation mechanism introduced by the cascaded X-shaped slots.

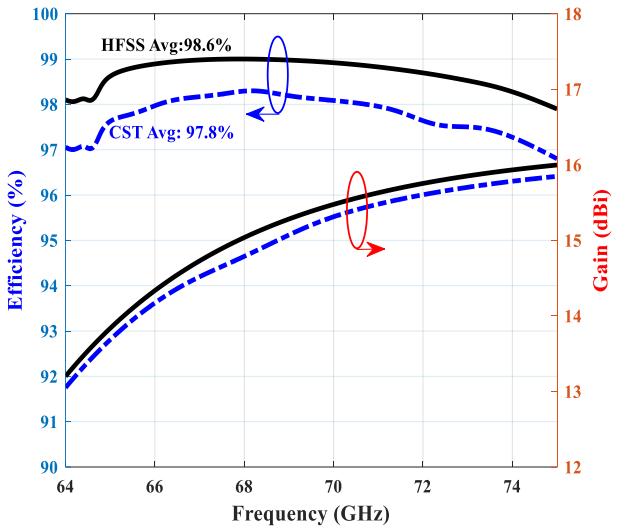

Fig. 10 Simulated radiation efficiency and realized gain of the proposed antenna obtained from HFSS and CST.

C. Frequency-Dependent Beam Scanning and Axial Ratio Performance

One of the key advantages of the proposed CP-PLWA is its frequency-controlled beam scanning capability. Fig. 8 shows the simulated normalized RHCP radiation patterns in the YZ plane at multiple frequencies across the 66–75 GHz band, together with the corresponding axial ratio (AR).

As the frequency increases, the main beam scans continuously from approximately −15° (backward region) at 66 GHz to +60° (forward region) at 75 GHz. This scanning behavior is in excellent agreement with the theoretical leaky-wave relation, Eq. (14), and is fully consistent with the dispersion diagram presented in Section III. Importantly, no open stopband is observed near broadside, which is a common limitation in many periodic leaky-wave antennas.

The axial ratio remains below 3 dB throughout the entire 66–75 GHz band, yielding a 3-dB AR bandwidth exceeding 13.6% (9 GHz). The minimum AR occurs near the main beam direction, indicating that high-quality circular polarization is maintained over the full scanning range.

To further validate the radiation characteristics, the three-dimensional radiation patterns of the proposed CP-PLWA at multiple frequencies are illustrated in Fig. 9. Fig. 9(a) shows the broadside radiation pattern at 67.15 GHz. Fig. 9(b) presents unnormalized (linear-scale) 3-D radiation patterns at 66, 67.15, 69, 71, and 73 GHz, clearly demonstrating directive radiation with a single dominant beam whose direction varies smoothly with frequency.

D. Gain and Radiation Efficiency

Fig. 10 presents the simulated realized gain and radiation efficiency of the proposed CP-PLWA as functions of frequency, obtained using HFSS and CST Microwave Studio.

As shown in Fig. 9, the realized gain increases gradually with frequency and remains above 13 dBi across the entire operating band (66–75 GHz), reaching a maximum value of approximately 16 dBi near the upper portion of the band. The gain variation over the operational bandwidth is less than 3 dB, indicating stable radiation performance during

TABLE I
Performance Comparison with state-of-the-art Leaky-Wave Antennas.

Ref	LWA Type	Freq. BW (GHz)	Scanning range (degree)	Max Gain (dBi)	Pol	3-dB CP BW (GHz)	Broadside Radiation	Max Radiation Effi.	Length / λ0
[16]	Dielectric Image Line	75–85 (11.3%)	18° (−8° to +10°)	12.7	**CP**	75–85 (11.3%)	Yes	Not Given	11.1
[17]	PCB based	57-66 (14.63%)	40◦ (-28◦ to +15◦)	17(sim.)	LP	____	Yes	87% (sim)	16
[18]	Circular series-fed patch array	79-81 (11.4%)	63◦ (-78◦ to -44◦) (27◦ to 42◦)	15	LP	____	No	85% (sim)	12.7
[19]	Bulky IDW (3D-printed)	50–75 (40%)	49° (−9° to +40°)	14.2	LP	–	Yes	75%	8.33
[20]	PPW-based CTS LWA + LCP	28.3–31.8 (11.7%)	108° (−56° to +52°)	**25.5**	**CP**	28.3–31.8 (11.7%)	Yes	>73.4% (meas.)	8.2
[22]	M-HMSIW (CELC loaded)	61.2-73.4 (18.3%)	50◦ (-25◦ to +25◦)	11.1	CP	64-70.8 (10.22%)	Yes	96.2% (sim)	3.8
This work	**CSRR-HMSIW (X-Shaped Slots)**	**64.4–77.75 (20.1%)**	**75° (−15° to +60°)**	**>13 (max 16)**	**CP**	**66–75 (13.6%)**	**Yes**	**>97% (sim.)**	**3.6**

backward-to-forward beam scanning. The radiation efficiency is also plotted in Fig. 10, demonstrating consistently high values throughout the band. The radiation efficiency, calculated as:

$$\eta_r = \frac{P_{rad}}{P_{accepted}} \quad (17)$$

remains above 97% for all frequencies, with average values of 98.6% and 97.8% obtained from HFSS and CST, respectively.

The close agreement between the two independent full-wave solvers confirms the numerical robustness of the results and highlights the low-loss nature of the proposed via-free CSRR-HMSIW leaky-wave structure.

IV. Comparison with State-of-the-Art Works

To validate the proposed design, Table I compares key performance metrics with recent mm-wave LWAs. As shown, many high-gain designs [17-19] are limited to linear polarization (LP), reducing their reliability in radar applications compared to CP solutions.

Conversely, CP counterparts often suffer from integration complexities or restricted fields of view. For instance, the dielectric image line (DIL) antenna in [16], while low-loss, exhibits a severely restricted scanning range of only 18° (−8◦ −8◦ to +10◦), limiting its utility in wide-angle tracking. Similarly, the volumetric parallel-plate waveguide structure in [20] precludes seamless integration with planar MMICs.

In contrast, the proposed work utilizes a fully planar, via-free architecture to achieve a wide continuous scanning range of 75° (-15° to +60°). Furthermore, compared to earlier planar CP attempts such as [22], the integration of the novel X-shaped slot topology in this design yields a decisive performance leap. This superior perturbation mechanism significantly enhances mode coupling, boosting the peak gain to 16 dBi and extending the 3-dB CP bandwidth to 13.6%. Combined with an exceptional simulated efficiency of >97%, this work offers the most robust trade-off between compactness, wideband CP performance, and scanning coverage among reported 70 GHz LWAs.

V. Fabrication Challenges and Practical Considerations

While this work is based on rigorous simulation validated across two independent solvers, practical realization at 70 GHz presents specific challenges that must be acknowledged.

1. **Critical Dimension Control**: The CSRR gaps and the fine features of the X-shaped slots require fabrication precision better than 10 μm. Standard PCB photolithography can achieve this, but process tolerance and etching uniformity become critical factors that can shift the operating frequency and affect CP performance.
2. **Substrate Parameter Stability:** The design is sensitive to the substrate's dielectric constant and thickness. Variations in these parameters, which can occur between substrate batches or due to temperature fluctuations, must be minimized. The use of a well-characterized, low-loss laminate like Rogers RT/duroid 5880 is essential.
3. **Measurement Infrastructure:** Experimental validation requires a Vector Network Analyzer (VNA) extending to at least 110 GHz for reliable S-parameter measurement. Far-field pattern and axial ratio characterization demands a precision millimeter-wave anechoic chamber with a capable positioner and a calibrated CP probe, which presents a significant infrastructure hurdle.

The strong agreement between HFSS and CST simulations for key metrics (impedance matching, broadside pattern) provides high confidence in the design's feasibility. This simulated performance serves as a critical benchmark, and addressing these fabrication and measurement challenges is the focus of ongoing work towards a physical prototype.

VI. Conclusion

This paper presents a novel, fully planar CP-PLWA for a 70 GHz millimeter-wave radar, featuring a wide axial ratio bandwidth and scanning range. A CSRR-HMSIW feed with integrated cascaded X-shaped slots enables controlled surface current perturbation for optimized circular polarization and backward-to-forward beam

scanning. Simulations show a 20.1% impedance bandwidth (64.4–77.75 GHz), exceeding 13.6% axial ratio bandwidth (AR < 3 dB), and a -15° to 60° scan angle. Gain exceeds 13 dBi (peaking at 16 dBi) with efficiency >97%. This compact, planar design offers a significant advancement in CP LWAs for 70 GHz radar.

ACKNOWLEDGMENTS

The author would like to express appreciation to all those who directly or indirectly contributed to this research work.

FUNDING STATEMENT

This research received no specific grant from any funding agency in the public, commercial, or not-for-profit sectors.

CONFLICTS OF INTEREST

The author declares that there is no conflict of interest regarding the publication of this article.

AUTHORS' CONTRIBUTIONS

Yalda Torabi is the sole author of this work. She was responsible for the conceptualization, design, simulation, data collection, analysis, interpretation, manuscript drafting, editing, and project administration.

STATEMENT ON THE USE OF GENERATIVE AI

The author used generative artificial intelligence tools solely for language editing and grammar correction purposes. All intellectual content, design, data, and interpretations are entirely the author’s original work, and the author takes full responsibility for the accuracy and integrity of the article.

REFERENCES

[1] S. Kiani, P. Rezaei, and M. Khajenoori, "Wideband sun-star shape coplanar waveguide antenna for terahertz sensing applications," *Results in Optics*, vol. 19, p. 100815, 2025/05/01/ 2025, doi: https://doi.org/10.1016/j.rio.2025.100815.

[2] S. Kiani, P. Rezaei, and M. Fakhr, "On-chip coronavirus shape antenna for wide band applications in terahertz band," *Journal of Optics*, vol. 52, pp. 860 - 867, 2023.

[3] P. Sohrabi, P. Rezaei, S. Kiani, and M. Fakhr, "A symmetrical SIW-based leaky-wave antenna with continuous beam scanning from backward-to-forward through broadside," *Wireless Networks*, vol. 27, 11/01 2021, doi: 10.1007/s11276-021-02798-6.

[4] Y. Banday, G. Mohammad Rather, and G. R. Begh, "Effect of atmospheric absorption on millimetre wave frequencies for 5G cellular networks," *IET Communications*, vol. 13, no. 3, pp. 265-270, 2019, doi: https://doi.org/10.1049/iet-com.2018.5044.

[5] W. Hong *et al.*, "The Role of Millimeter-Wave Technologies in 5G/6G Wireless Communications," *IEEE Journal of Microwaves*, vol. 1, pp. 101-122, 01/01 2021, doi: 10.1109/JMW.2020.3035541.

[6] X. Huo and Z. Li, "Circularly Polarized Leaky-Wave Antenna Based on Low-Loss Transmission Line," *International Journal of Antennas and Propagation*, vol. 2022, no. 1, p. 7224725, 2022, doi: https://doi.org/10.1155/2022/7224725.

[7] H. Lee, J. H. Choi, C. T. M. Wu, and T. Itoh, "A Compact Single Radiator CRLH-Inspired Circularly Polarized Leaky-Wave Antenna Based on Substrate-Integrated Waveguide," *IEEE Transactions on Antennas and Propagation*, vol. 63, no. 10, pp. 4566-4572, 2015, doi: 10.1109/TAP.2015.2456935.

[8] P. N. Choubey, X. Zhang, T. He, N. Hao, and K. Xu, "Substrate Integrated Waveguide Based Cavity-Backed Circularly-Polarized Antenna for Satellite Communication," *Electronics*, vol. 12, no. 7, p. 1669, 2023. [Online]. Available: https://www.mdpi.com/2079-9292/12/7/1669.

[9] X. Li, J. Wang, G. Goussetis, and L. Wang, "Circularly Polarized High Gain Leaky-Wave Antenna for CubeSat Communication," *IEEE Transactions on Antennas and Propagation*, vol. 70, no. 9, pp. 7612-7624, 2022, doi: 10.1109/TAP.2022.3167773.

[10] A. P. Saghati, M. M. Mirsalehi, and M. H. Neshati, "A HMSIW Circularly Polarized Leaky-Wave Antenna With Backward, Broadside, and Forward Radiation," *IEEE Antennas and Wireless Propagation Letters*, vol. 13, pp. 451-454, 2014, doi: 10.1109/LAWP.2014.2309557.

[11] D. Deslandes and K. Wu, "Single-substrate integration technique of planar circuits and waveguide filters," *IEEE Transactions on Microwave Theory and Techniques*, vol. 51, pp. 593-596, 2003.

[12] D. R. Jackson, C. Caloz, and T. Itoh, "Leaky-Wave Antennas," *Proceedings of the IEEE*, vol. 100, no. 7, pp. 2194-2206, 2012, doi: 10.1109/JPROC.2012.2187410.

[13] F. Monticone and A. Alù, "Leaky-Wave Theory, Techniques, and Applications: From Microwaves to Visible Frequencies," *Proceedings of the IEEE*, vol. 103, no. 5, pp. 793-821, 2015, doi: 10.1109/JPROC.2015.2399419.

[14] J. Xu, W. Hong, H. Tang, Z. Kuai, and K. Wu, "Half-Mode Substrate Integrated Waveguide (HMSIW) Leaky-Wave Antenna for Millimeter-Wave Applications," *IEEE Antennas and Wireless Propagation Letters*, vol. 7, pp. 85-88, 2008, doi: 10.1109/LAWP.2008.919353.

[15] Y. Dong and T. Itoh, "Composite Right/Left-Handed Substrate Integrated Waveguide and Half Mode Substrate Integrated Waveguide Leaky-Wave Structures," *IEEE Transactions on Antennas and Propagation*, vol. 59, pp. 767-775, 2011.

[16] A. Zandamela, A. Al-Bassam, and D. Heberling, "Circularly Polarized Periodic Leaky-Wave Antenna Based on Dielectric Image Line for Millimeter-Wave Radar Applications," *IEEE Antennas and Wireless Propagation Letters*, vol. PP, pp. 1-1, 03/19 2021, doi: 10.1109/LAWP.2021.3067496.

[17] M. Steeg, B. Khani, V. Rymanov, and A. Stöhr, "Novel 50–70 GHz compact PCB leaky-wave antenna with high broadside efficiency and low return loss," presented at the 2016 41st International Conference on Infrared, Millimeter, and Terahertz Waves (IRMMW-THz), Copenhagen, Denmark, 2016.

[18] H. Aliakbari, M. Mosalanejad, C. Soens, G. A. E. Vandenbosch, and B. K. Lau, "79 GHz Multilayer Series-Fed Patch Antenna Array With Stacked Micro-Via Loading," *IEEE Antennas and Wireless Propagation Letters*, vol. 21, no. 10, pp. 1990-1994, 2022, doi: 10.1109/LAWP.2022.3187764.

[19] X. Bai, S. W. Qu, K. B. Ng, and C. H. Chan, "Sinusoidally Modulated Leaky-Wave Antenna for Millimeter-Wave Application," *IEEE Transactions on Antennas and Propagation*, vol. 64, no. 3, pp. 849-855, 2016.

[20] Q. D. Cao, X. X. Yang, F. Yu, and S. Gao, "High Scanning Rate Millimeter-Wave Circularly Polarized CTS Leaky Wave Antenna," *IEEE Transactions on Antennas and Propagation*, vol. 72, no. 7, pp. 6087-6092, 2024, doi: 10.1109/TAP.2024.3349674.

[21] M. Nitas, M.-T. Passia, and T. V. Yioultsis, "Fully planar slow-wave substrate integrated waveguide based on broadside-coupled complementary split ring resonators for mmWave and 5G components," *IET Microwaves, Antennas & Propagation*, vol. 14, no. 10, pp. 1096-1107, 2020, doi: https://doi.org/10.1049/iet-map.2019.1014.

[22] Y. Torabi, H. Oraizi, A. Araghi, and M. Khalily, "Miniaturized V-band circularly polarized leaky-wave antenna with continuous radiation coverage using modified waveguide and metasurface CSRRs," *Scientific Reports*, vol. 13, no. 1, p. 10162, 2023/06/22 2023, doi: 10.1038/s41598-023-37362-z.

[23] A. Parsa, P. Rezaei, A. AmneElahi, A. Khatami, and Z. Mousavirazi, "Efficient transition from SMA to ESIW for planar slot array antennas in wireless systems," *Analog Integrated Circuits and Signal Processing*, vol. 125, no. 1, p. 18, 2025/09/11 2025, doi: 10.1007/s10470-025-02498-7.

[24] D. M. Pozar, *Microwave Engineering*. Wiley, 2012.

[25] M. Bozzi, A. Georgiadis, and K. Wu, "Review of substrate integrated waveguide circuits and antennas," *IET Microwaves, Antennas & Propagation*, vol. 5, no. 8, pp. 909-920, 2009, doi: 10.1049/iet-map.2009.0463.

[26] W. Hong, Y. D. Cheng, and K. Wu, "Half mode substrate integrated waveguide: Analysis and applications," *IEEE Transactions on Microwave Theory and Techniques*, vol. 54, no. 1, pp. 298-306, 2006, doi: 10.1109/TMTT.2005.860274.

[27] E. Hammerstad and O. Jensen, "Accurate models for microstrip computer-aided design," *IEEE MTT-S International Microwave Symposium Digest*, pp. 407-409, 1980.

[28] J. D. Baena, R. Marqués, F. Medina, and J. Martel, "Equivalent-circuit models for split-ring resonators and complementary split-ring resonators," *IEEE Transactions on Microwave Theory and Techniques*, vol. 53, no. 4, pp. 1451-1461, 2005, doi: 10.1109/TMTT.2005.845211.

[29] F. W. Grover, *Inductance Calculations: Working Formulas and Tables*. New York: Dover Publications, 1946.

[30] R. Marqués, F. Martín, and M. Sorolla, *Metamaterials with Negative Parameters: Theory, Design, and Microwave Applications*. Hoboken,

NJ, USA: Wiley, 2008.
[31] C. Caloz and T. Itoh, *Electromagnetic Metamaterials: Transmission Line Theory and Microwave Applications.* Hoboken, NJ: Wiley-IEEE Press, 2006.